Open Access Tools for the Simulation of Ultrashort-Pulse Laser Ablation

Stefan Scharring[a], Daniel J. Förster[a], Hans-Albert Eckel[a], Johannes Roth[b], and Mikhail Povarnitsyn[c]

[a]*Institute of Technical Physics, German Aerospace Center (DLR), Pfaffenwaldring 38 – 40, 70569 Stuttgart, Germany*
[b]*Institute of Functional Materials and Quantum Technologies (FMQ), Pfaffenwaldring 57, University of Stuttgart, 70569 Stuttgart, Germany*
[c]*Joint Institute for High Temperatures, Russian Academy of Sciences (RAS), Izhorskaya st. 13 Bd. 2, Moscow, Russia 125412*

Abstract. A comparison is given on the simulation of laser ablation using two completely different approaches which are freely available online. Virtual Laser Laboratory (VLL) from RAS is based on a hydrodynamic code accessible online by a graphical user interface. Simulations on laser ablation, based on the Two-Temperature-Model (TTM) are carried out rapidly allowing for extended parameter studies. On the other hand, IMD from FMQ is an open source code for molecular dynamics for a wide range of applications in solid state physics including laser ablation. Laser material heating is supported in two ways, either by simple energy rescaling of the material (RES model) or by usage of the TTM which is implemented as well. Simulation results from VLL and IMD for laser heating, melting and ablation of aluminum by ultrashort laser pulses are compared and discussed with respect to density and temperature distributions, phase transitions, plume propagation and ionization. Simulation performance is evaluated and limitations with respect to optical parameters, especially pulse length scaling, and sample dimensionality are discussed.

Keywords: Laser ablation, Ultrashort laser pulses, Two-Temperature model, hydrodynamic simulation, Molecular dynamics, Plume propagation, Impulse coupling coefficient, Specific impulse

PACS: 02.70.Ns, 42.55.-f, 44.05.+e, 47.11.Fg, 64.30.Ef, 79.20.Ds, 89.20.Hh

1. INTRODUCTION

The simulation of laser-induced ablation of metals by numerical methods is investigated by various research groups in the scientific community. The choice of the simulation method is strongly dependent on scaling issues, e.g. size of the simulation elements (atoms, meso-scalic particles, fluid cells), sample dimension, required time step, laser intensity range and pulse length. The extensive effort for the development of a model that mirrors the physical reality adequately is obvious.

Several commercial available computational codes exist which are intended or at least suitable to model laser ablation, e.g. MACH2 [1], EMSolve [2], MAGIC3D, and LSP [3] while on the other hand open source codes can be found that allow for the

implementation of modules for laser-matter interaction, e.g. DEM codes like LAMPPS [4] or FEM codes like openFOAM [5].

Open-source codes that can already deal with phenomena related to laser ablation provide for a good introduction into the development of own simulation tools that are suitable for specific questions of a research topic. Moreover, parameter studies for the application of laser ablation can be carried out more or less easily.

Aiming for parameter studies for laser ablative micro propulsion and laser-based space debris removal, at DLR Stuttgart, two very different open-source simulation tools for laser-ablation have been employed. In this paper, a short comparative summary is given on these programs, Virtual Laser Lab (VLL), a hydrodynamic code for online simulations [6] developed at the Joint Institute for High Temperatures RAS, Moscow, and IMD, a molecular dynamic code [7,8,9] developed at the FMQ, formerly: ITAP, University of Stuttgart. A preliminary comparison was given in [10].

2. THEORETICAL BACKGROUND

A. Two-Temperature Model

Energy deposition by an ultrafast laser pulse into a metal target can be described by the Two-Temperature Model (TTM) according to [11] by

$$\boldsymbol{c_e(T_e)\frac{\partial T_e}{\partial t} = \nabla[\kappa_e(T_e)\nabla T_e] - \gamma_{ei}(T_e - T_i) + S(\vec{r}, t)} \tag{1}$$

$$\boldsymbol{c_i(T_i)\frac{\partial T_i}{\partial t} = \nabla[\kappa_i(T_i)\nabla T_i] + \gamma_{ei}(T_e - T_i)} \tag{2}$$

where the indices e and i denote the electron and ionic subsystem, resp., c is the specific heat capacity, T the temperature, κ represents the thermal conductivity, and γ_{ei} is the electron-phonon coupling parameter. Following [12], κ_i can be neglected for ultrashort laser pulses, as it is done in VLL and IMD. Hence, simulation results of VLL (and IMD) of ablation events by pulses in the nanosecond regime would exhibit a limited validity.

B. Hydrodynamic Simulation - VLL

According to [13], where a sound description of the specific simulation assumptions in VLL is given, laser-matter interaction is described here by the TTM in a single-fluid 1D Lagrangian form yielding a modification of Eq. 1 and 2 by

$$\boldsymbol{\frac{\partial e_e}{\partial t} + P_e\frac{\partial u}{\partial m} = \frac{\partial}{\partial m}\left[\varrho\kappa_e\frac{\partial T_e}{\partial m}\right] - \gamma_{ei}(T_e - T_i)/\varrho + S(x, t)/\varrho} \tag{3}$$

$$\boldsymbol{\frac{\partial e_i}{\partial t} + P_i\frac{\partial u}{\partial m} = +\gamma_{ei}(T_e - T_i)/\varrho,} \tag{4}$$

where e_e and e_i denote the specific energy of the electrons and ions, resp., P is the pressure, m mass, ϱ density, and, in contrast to [13], radiation transport phenomena are neglected here. The underlying data for the dependency of κ_e and γ_{ei} from T_e are taken from a wide-range model given in [14]. Conservation of mass and energy are granted using

$$\frac{\partial(1/\varrho)}{\partial t} - \frac{\partial u}{\partial m} = 0, \tag{5}$$

$$\frac{\partial u}{\partial t} + \frac{\partial(P_i + P_e)}{\partial m} = 0. \tag{6}$$

This set of equations can be solved for ϱ, T_e, T_i using semi-empirical two-temperature multiphase equations of state (EOS) yielding $P_e(\varrho, T_e)$, $e_e(\varrho, T_e)$, $P_i(\varrho, T_i)$, and $e_i(\varrho, T_i)$ for aluminum, as described in greater detail in [13] and the related literature. Hence, apart from the above mentioned quantities, phase state and, moreover, equilibrium mean charge of ions $\langle Z \rangle$ is given as output from the simulation. Whereas we restrict on simulations with aluminum targets here, it should be noted that calculations for silver and gold as well as water, nitrogen, and argon are feasible in VLL as well.

The temporal course of incident laser radiation is given by an analytical expression $I(t)$, multiple pulses are supported and can be applied as well.

C. Molecular Dynamics Simulation – IMD

In IMD, as a Molecular Dynamics simulation code, atoms or molecules, resp., interact via potentials. In the case of aluminum, we have chosen an embedded atom potential based on a local electron density as given in [15]. The TTM according to Eq. 1, however, is implemented in IMD as an additional "layer" of cells where the corresponding equation is solved in a finite-differences (FD) approach. Interaction of FD cells and MD cells is performed in very short timesteps, as described below.

In contrast to VLL, γ_{ei} and κ_e are set as constant parameters, $\gamma_{ei} = 5.69 \cdot 10^{17}\ \mathrm{J/(s \cdot m^3 \cdot K)}$ [16], $\kappa_e = 235\ \mathrm{J/(s \cdot m \cdot K)}$ [12], and their dependency from T_e is neglected. For the electron heat capacity, a linear approximation is undertaken, $c_e(T_e) = 135\,\mathrm{J/(m^3 K^2)} \cdot T_e$, [17] which is applicable, if T_e is far below the Fermi temperature [12].

An extensive description on IMD with respect to the ablation of metals is given in [18, 19, 20].

D. Simulation setup

1. Sample material

Since the dimension of the simulation cells in VLL is in the nanometer range and therefore rather large, it is not disadvantageous with respect to the computational effort to create bulk material with a certain thickness, which was chosen as 1 mm here.

The shockwave stemming from the ablation event is supposed to travel with the corresponding speed of sound and will have no impact on the rear side of the target within the simulation time t_{sim}.

In IMD, however, computational time scales linearly with the number of particles. With VLL results as an orientating guideline for sample dimensionality, samples with a thickness in the range of 500 nm to 650 nm have been created. 20 nm have been chosen as lateral extension using periodic boundary conditions [10]. As it can be seen from Fig. 1, in the case of long simulation times, reflection of the shockwave at the rear side of the target occurs which is accompanied by spallation. In order to simulate a bulk target however, a ramp can be introduced that absorbs energy by cooling down the atoms in the deeper levels of the target.

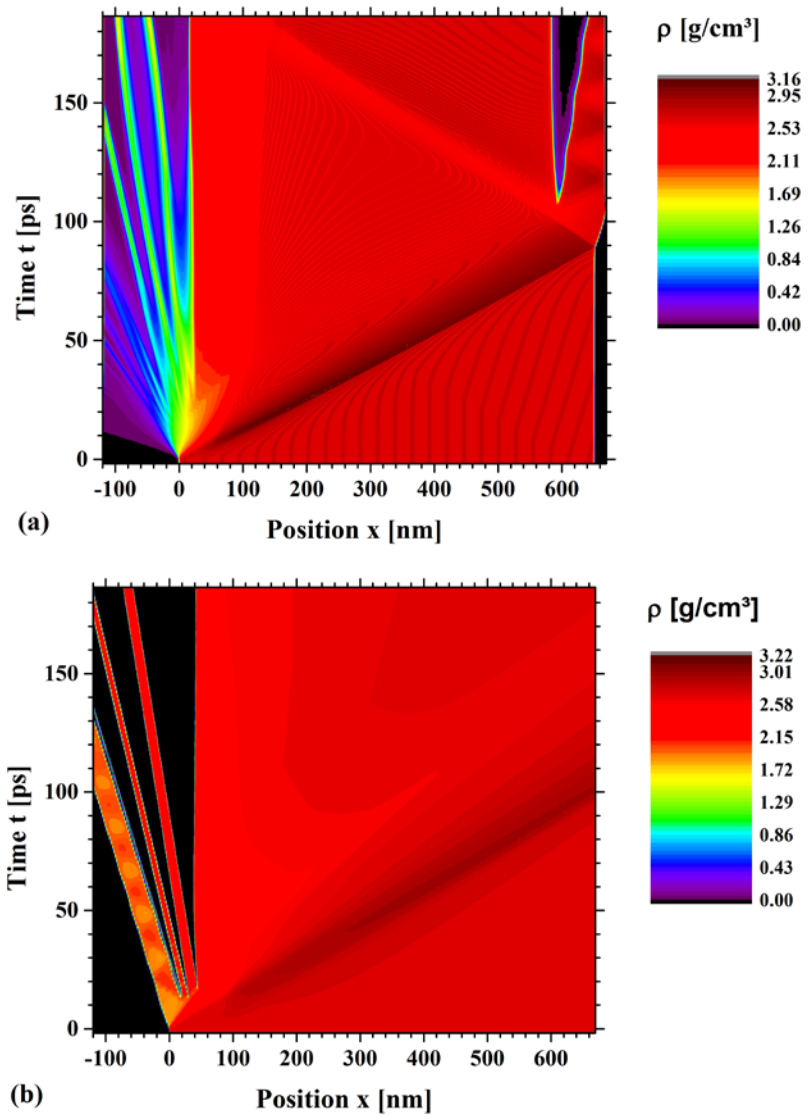

FIGURE 1. Density plots – Results from (a) IMD simulations with a thin target ($\boldsymbol{d = 650\ nm}$) and (b) VLL simulations with a bulk target ($\boldsymbol{d = 1\ mm}$).
Simulation parameters: $\boldsymbol{\tau \approx 500\ fs}$, $\boldsymbol{\Phi_L = 0.74\ J/cm^2}$, $\boldsymbol{\Phi_{abs} = 0.078\ J/cm^2}$.

2. Laser-matter interaction

In the VLL simulations, the temporal course of the laser pulse intensity was given by

$$\mathbf{I}(\boldsymbol{t}) = \boldsymbol{I_0} \cdot \mathbf{exp}\left[-\frac{\boldsymbol{t^2}}{\mathbf{2}\boldsymbol{\sigma_t}}\right] \tag{7}$$

with

$$\boldsymbol{I_0} = \frac{\boldsymbol{\Phi_L}}{\mathbf{2.507}\cdot\boldsymbol{\sigma_t}\cdot\mathbf{cos}\,\boldsymbol{\vartheta}} \tag{8}.$$

where Φ_L is the incident laser fluence and ϑ is the incidence angle. In the following, we denote the pulse length the full width half maximum (FWHM) with $\tau = \tau_{FWHM} = 2\sqrt{2\ln 2}\,\sigma_t$. With respect to our related work on laser micro propulsion and debris removal, $\lambda = 1064$ nm as laser wavelength and, for the sake of simplicity, an incidence angle of $\vartheta = 0°$ was chosen. For simulations with IMD the amount of absorbed energy intermediated by incident laser light has to be calculated beforehand. (Future developments will take this drawback into account.) It is worth to mention, however, that VLL can treat any incidence angle and polarization as well, and the laser wavelength can be chosen in the range from 200 nm to 2 µm.

In VLL, solutions of the Helmholtz equation in the simulation cells yield the temporal course of absorbed and reflected energy, cf. Fig. 2, which makes it a suitable tool for simulation of pump-probe experiments [14]. In contrast, the Lambert-Beer law is applied in IMD with a constant absorption coefficient $\alpha = 10^6\ cm^{-1}$, which was taken from [12].

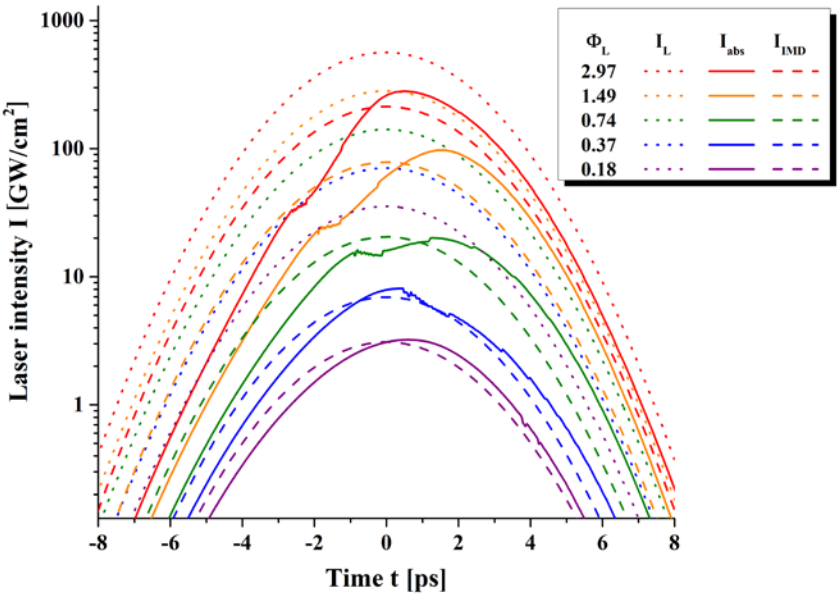

FIGURE 2. VLL results: Temporal courses of incident (dotted lines) and absorbed (solid lines) laser intensity for various fluences, given in J/cm², at $\boldsymbol{\tau = 2.1\ ps}$. The dashed lines indicate the courses of laser intensity that was used for comparative IMD simulations.

Hence, the overall absorbed fluence Φ_{abs}, as calculated in VLL, is taken as input parameter for the IMD simulations, since in IMD the reflectivity is assumed to be constant during the ablation, cf. Table 1. Though this is correct for pulses in the fs-

range, this assumption fails for longer laser pulses and/or very high fluences. For the temporal course of the laser pulse, a Gaussian shape is assumed in IMD. Fig. 2 shows the corresponding temporal courses of incident and absorbed laser intensity in VLL and IMD.

TABLE 1. Simulation parameters: Incident laser fluence $\boldsymbol{\Phi_L}$ and pulse length $\boldsymbol{\tau}$. Absorbed laser fluence $\boldsymbol{\Phi_{abs}}$ and accordingly reflectivity $\boldsymbol{R}$ during the ablation process was derived from VLL simulations. IMD Simulation results: Initial and final point in time of the simulation, Number of used CPUs $\boldsymbol{N_{CPU}}$, simulation time step $\boldsymbol{\Delta t}$, extension of the target x_t, extension of the simulation box x_b including vacuum, calculation time $\boldsymbol{t_{calc}}$, and specific simulation power P_s. For simulations marked with an asterisk, the calculation yielded unphysical results after t_{end}, see section 3.B.

$\boldsymbol{\Phi_L}$	$\boldsymbol{\tau}$	$\boldsymbol{\Phi_{abs}}$	$\boldsymbol{R}$	$\boldsymbol{t_{init}}$	$\boldsymbol{t_{end}}$	$\boldsymbol{N_{CPU}}$	$\boldsymbol{\Delta t}$	$\boldsymbol{x_t}$	$\boldsymbol{x_b}$	$\boldsymbol{t_{calc}}$	$\boldsymbol{P_s}$
$\boldsymbol{J/cm^2}$	$\boldsymbol{ps}$	$\boldsymbol{J/cm^2}$	$-$	$\boldsymbol{ps}$	$\boldsymbol{ps}$	$-$	$\boldsymbol{fs}$	$\boldsymbol{nm}$	$\boldsymbol{nm}$	$\boldsymbol{dd{:}hh}$	$\boldsymbol{ps \cdot nm/d}$
0.19	0.05	0.012	0.935	-0.204	51.613	8	1.018	400	500	5:22	546
0.37	0.05	0.028	0.925	-0.204	68.511	4	1.018	500	600	14:21	694
0.74	0.05	0.077	0.896	-0.204	97.626	8	1.018	650	790	21:00	460
1.49	0.05	0.249	0.832	-0.204	58.840	192	1.018	750	1400	1	446
2.97	0.05	0.766	0.742	-0.204	4.876*	256	0.1018	850	1490	0:09	113
0.19	0.5	0.013	0.93	-1.731	49.882	8	1.018	400	500	5:22	544
0.37	0.5	0.030	0.919	-1.731	66.577	4	1.018	500	600	14:21	690
0.74	0.5	0.078	0.895	-1.731	95.488	8	1.018	650	790	21:01	457
1.49	0.5	0.238	0.840	-1.731	42.043	128	1.018	750	1400	1	497
2.97	0.5	0.718	0.758	-1.018	4.062*	256	0.1018	850	1490	0:09	106
0.19	5	0.016	0.913	-15.779	36.241	8	1.018	400	500	5:11	547
0.37	5	0.037	0.902	-16.288	51.511	4	1.018	500	600	14:21	684
0.74	5	0.108	0.855	-16.288	65.050	8	1.018	650	950	21:00	460
1.49	5	0.413	0.722	-8.144	5.541*	192	1.018	750	1400	n.d.	n.d.
2.97	5	1.122	0.622	-17.306	2.952*	192	1.018	850	1490	n.d.	n.d.

3. RESULTS AND DISCUSSION

A. Computational performance

Though both VLL and IMD operate with a computational time step in the femtosecond range during the laser pulse, computational time is significantly diminished in VLL by increasing the timestep up to $\Delta t_{VLL} = 100$ fs after the pulse. Moreover, VLL operates with rather large hydrodynamic cells in the nanometer range. Hence, each simulation was finished after a few minutes and was carried online at [6].

Owing to the trajectory calculation of each particle in IMD with a fixed time step of around $\Delta t_{MD} = 1\ fs$, the simulation time is considerably larger, as shown in Table 1. Basically, transition to a moderately larger time step is possible after restart of the simulation of a certain checkpoint in time. However, the TTM part of the calculation cannot be restarted. The specific simulation power P_s for one CPU with

$$P_s = \frac{t_{sim} \cdot x_b}{N_{CPU} \cdot t_{calc}} \tag{9}$$

is shown in Table 1 as well. P_s mainly depends on the evenness of the particle distribution over the spatially fixed CPUs, the selected timestep, and the chosen compiling options of the code. It should be noted here that t_s would increase quadratically with the lateral extension of the sample.

MD-Simulations with $\Phi_L < 1 J/cm^2$ were carried out at DLR whereas ablation under higher fluences were computed at the High Performance Computing Center (HLRS) of the University of Stuttgart.

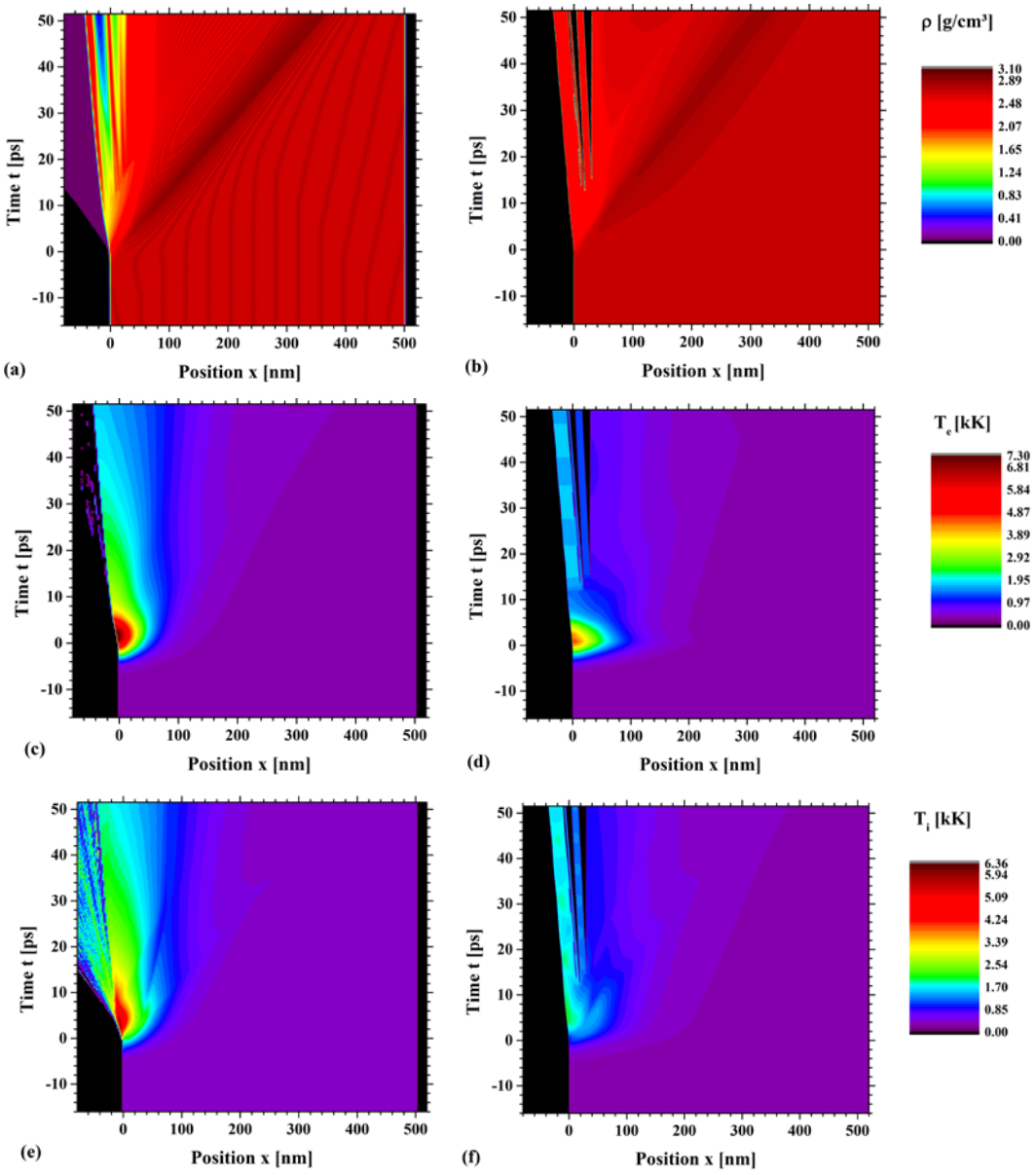

FIGURE 3. Results from Molecular Dynamics (IMD – (a), (c), (e)) and hydrodynamic simulation (VLL – (b), (d), (f)): (a),(b) Temporal and spatial distribution density ρ, (c),(d) electron temperature T_e, and (e),(f) ion temperature T_i of an aluminum target during ablation with a short laser pulse (τ = 5 ps, Φ_L = 0.37 J/cm², Φ_{abs} = 0.037 J/cm²).

B. Density and temperature

Since density and temperature are main variables for which the TTM equations are solved, sample plots of their distribution as calculated from VLL and IMD are shown in Fig. 3. At a first glance, density distributions of all simulations listed in Table 1 show a moderate similarity when the laser fluence is slightly above the ablation threshold, i.e. $\Phi_L \geq 0.74\ \mathrm{J/cm^2}$ @ 5 ps and $\Phi_L \geq 0.37\ \mathrm{J/cm^2}$ @ 50 fs, 500 fs. At short pulses at low fluence, however, VLL results indicated only melting of the sample, whereas ablation is shown in the IMD results. This can partly be ascribed to the differences in the assumptions of electron thermal conductivity and electron-phonon coupling between both models. Whereas the constant value of κ_e in IMD is in agreement with the wide-range model of VLL for $T_e \leq 5$ kK, in VLL κ_e increases slightly for higher electron temperatures. This supports a broadening of the heat affected zone and counteracts extreme high temperatures in the ionic subsystem, compared to IMD. However, one major reason for the significantly high ionic temperatures in IMD, leading to a lower ablation threshold, might be found in γ_{ei} which exceeds the wide-range model by a factor of 1.6 to 2.3 yielding a faster and spatially more confined energy transport to the ionic subsystem. In both codes, a linear approximation $c_e(T_e) = k_e T_e$ is applied, where the electron heat capacity coefficient of IMD, $k_e = 135\,\mathrm{J/(m^3K^2)}$, exceeds the one of VLL, $k_e \approx 100\,\mathrm{J/(m^3K^2)}$ which corresponds to the underlying EOS applied there.

Of course, the higher temperatures found from IMD simulations result in a lower threshold fluence for melting (onset at ~ 0.37 J/cm² from VLL, and at ~ 0.19 J/cm² from IMD @ 500 fs pulse length) and ablation (onset at ~ 1.49 J/cm² from VLL, and at ~ 0.37 J/cm² from IMD @ 500 fs pulse length).

In general, however, it should be considered that the potential [15] chosen in these MD simulations was developed for states adjacent to the normal state, i.e. at low pressure up to the melting temperature. Extreme conditions, however, where exited electrons have a significant impact on changes in atomic binding, are not taken into account but might yield considerable deviations. This comes apparent with simulations at fluences which are marked with an asterisk in Table 1. In this case, the atoms came that close to each other that the corresponding distance was in the interpolation range of the underlying EAM potential whereas extrapolation to lower distances might be doubtful from a physical point of view.

C. Ionization

In IMD simulations, it can be seen that the temperatures of both the electronic and the ionic subsystem are about a factor 2 – 4 higher than in VLL simulations. As ionization is not taken into account in IMD simulations, energy transport between electronic and ionic system is mediated by TTM equations (1,2) and partially by interatomic potentials. Energy is not absorbed by the process of ionization itself, so in total a higher amount of energy has an impact on the particle motion, i.e. their kinetic energy, than in VLL simulations or common sense expectation. This also may be a reason for simulations at higher fluences to abort at the same simulation time step. Energy expected to result in partially ionized species is redistributed on the sample,

leading to steeper rise of energy stored in the electronic system, leading to more energy exchange between electronic and ionic systems, resulting in the need for shorter simulation time steps in order to resolve particle movement. Limitations in this case arise from the tabulated potentials, as already mentioned above, which are only given to a certain distance minimum of two particles interacting with each other.

However, the missing implementation of ionization in IMD appears not to be the only reason for these large discrepancies, since e.g. at Φ_L = 1.49 J/cm², VLL simulations show that only a fraction of ~ 5 – 10 % of the incident laser energy yields ionization. Nevertheless, since equilibrium values of ⟨Z⟩ are given in VLL, this energy fraction might in fact be higher in ultrafast dynamics. For a more detailed analysis, the underlying EOS of VLL would have to be compared with those which can be deduced from the potential used in IMD.

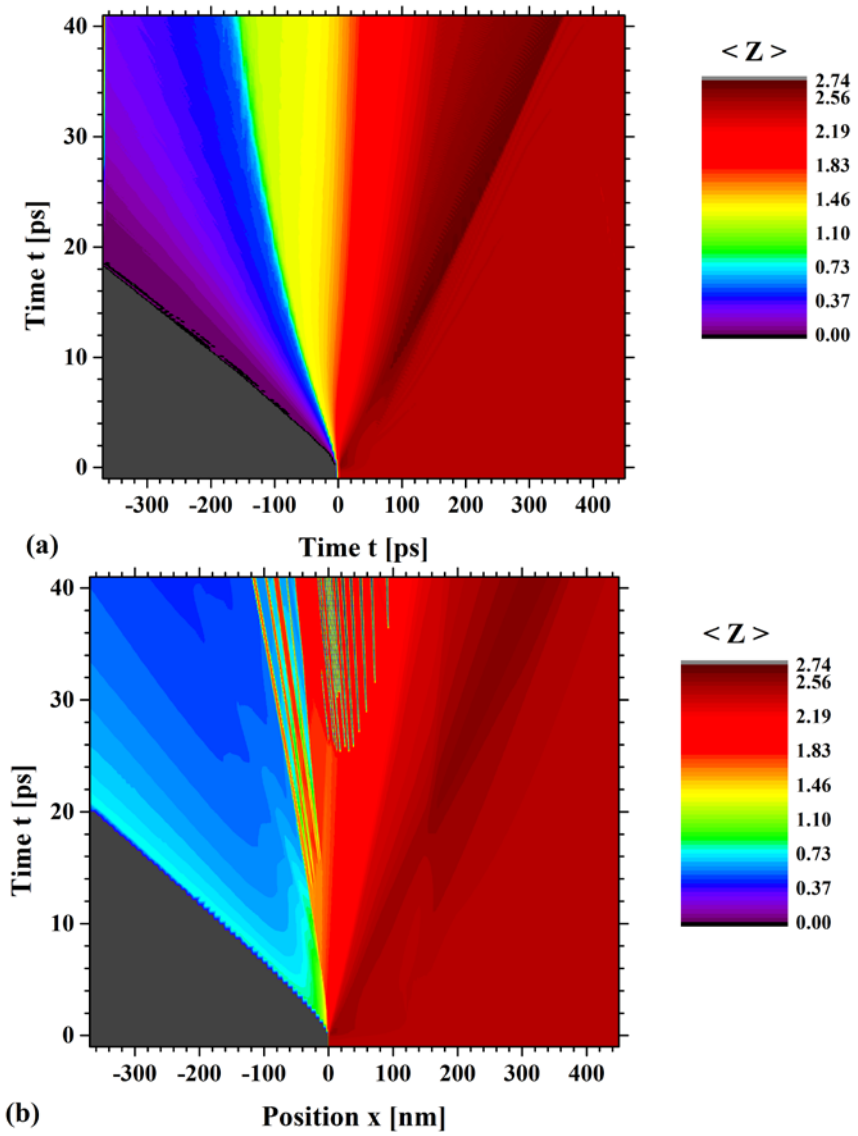

FIGURE 4. (a) Mean charge <Z> corresponding to the IMD results according to [21] and (b) <Z> from VLL calculations for τ = 500 fs and Φ_L = 1.49 J/cm².

Basically, the plasma state is not taken into account in IMD simulations whereas it is integrated in the EOS of VLL. For comparison, however, the mean charge was calculated from IMD results that would correspond to the IMD data of ρ and T_e according to the equations in [21]. These equations are equivalent to the consideration of ionization in the EOS of VLL. Again, it should be noted, that Fig. 4(a) serves only for orientation, since the implementation of ionization into the EAM potentials used in IMD should yield lower values of T_e since energy is required for ionization.

D. Jet propagation

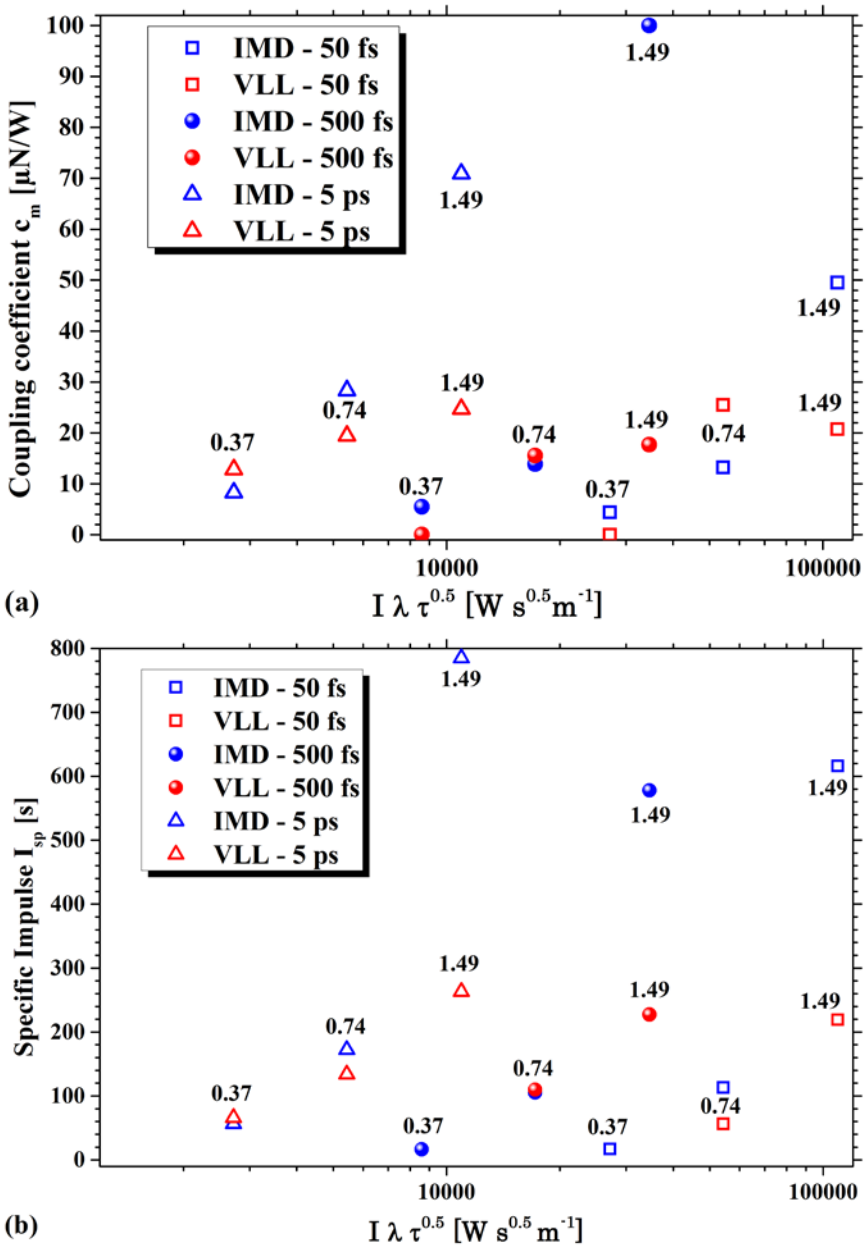

FIGURE 5. Comparison of (a) coupling coefficient and (b) specific impulse from simulation data of VLL and IMD for various pulse lengths at incident laser fluences as labeled in the graphs in J/cm².

As an application for laser ablative micro propulsion, momentum coupling was derived from the ablation plume. Momentum conservation yields impulse transfer to the target which might serve as an impulse bit under repetitive operation in a micro-thruster. The temporal course overall momentum p of the ablation plume ($x < 0$) was derived and analyzed with respect to its asymptotic value after the ablation event. The weight-averaged velocity $\langle v \rangle$ of the jet was calculated this way as well. For a comparison of both simulations, however, Fig. 5 shows common figures of merit in laser propulsion, the impulse coupling coefficient c_m and the specific impulse I_{sp} vs. the well-established scaling parameter $I\lambda\sqrt{\tau}$ [23], where $c_m = p/\Phi_L$ and $I_{sp} = \langle v \rangle / g$, where g is the gravitational constant.

Apart from different findings for the ablation threshold in the simulations, results for c_m and I_{sp} are in the same order of magnitude at lower fluences, regardless of the pulse length. Comparison with experimental data from [22] ($c_m = 18\ \mu N/W\ @\ \Phi_L = 1.17\ J/cm^2, \lambda = 800\ nm, \tau = 130\ fs$) indicates generally the agreement with physical reality. However, with higher fluences, namely $\Phi_L = 1.49\ J/cm^2$, IMD results for c_m significantly exceed the values obtained from VLL. This may primary not be attributed to differences in ablated mass, but to much higher jet velocities, cf. Fig. 5 b). One reason can be seen in the onset of plasma formation which is considered in the calculations of VLL. In IMD, however, the fraction of laser energy which would serve as ionization energy is treated as kinetic energy.

4. CONCLUSIONS

Since IMD is an open-source code, many extensions are possible, e.g. the implementation of the temperature dependency of electron thermal conductivity, electron-phonon coupling and surface reflectivity. The setup of an ionization module taking into account for corresponding losses in kinetic energy during the simulation is recommended for higher fluences and longer pulses as well. In general, for longer pulses it should be considered whether the extended Two-Temperature-Model (eTTM) might yield more realistic results for both simulation codes [24].

The computational extension towards 2D laser spots yielding 3D ablation craters would be highly desirable. Basically, 2D laser spots can already be calculated in IMD with 3D targets. However, realistic spot sizes in the range of several micrometers require a considerable effort with respect to parallelization and required computational time. Nevertheless, results in the nm-range show remarkable agreements with meso-scalic experimental findings [19]. It might be instructive to extend the comparison of open-source codes for ultra-short pulse laser ablation on MULTI-fs [25]. Moreover, for longer pulses the hydrodynamic code MULTI can be applied [26].

ACKNOWLEDGMENTS

Financial funding by SFB 716 “Dynamic simulation of systems with large particle numbers”, University of Stuttgart, and the allocation of computational time at the High Performance Computing Center (HLRS) of the University of Stuttgart are greatly acknowledged.

REFERENCES

1. T. Moeller, Y.K. Chang, “MACH2 simulations of a micro laser ablation plasma thruster”, Aerospace Science and Technology, vol. 11, pp. 481–489 (2007).
2. A. Heller, “A Code to Model Electromagnetic Phenomena”, Science & Technological Review, vol. 11, pp. 4 – 10 (2007).
3. A.J. Woods and L.D. Ludeking, “MAGIC Electromagnetic FDTD-PIC Code Dense Plasma Model Comparison with LSP”, The Open Plasma Physics Journal, vol. 3, 73–77 (2010).
4. Starikov et al., “Laser Ablation of Gold: Experiment and Atomistic Simulation”, JETP Letters, vol. 93(11), 642–647 (2011)
5. Leitz et al., “Numerical simulation of process dynamics during laser beam drilling with short pulses”, Applied Physics A, vol. 106, pp. 885–891 (2012).
6. Online Simulations accessible at http://vll.ihed.ras.ru/
7. Available online at http://imd.itap.physik.uni-stuttgart.de/
8. J. Roth, F. Gähler, and H.-R. Trebin, “A molecular dynamics run with 5 180 116 000 particles”, *Int. J. Mod. Phys. C.* **11**: 317 – 322 (2000).
9. J. Stadler, R. Mikulla, and H.-R. Trebin, “IMD: A Software, Package for Molecular Dynamics Studies on Parallel Computers”, *Int. J. Mod. Phys. C* **8**: 1131 – 1140 (1997).
10. D.J. Förster, “Validation of the software package IMD for molecular dynamics simulations of laser induced ablation for micro propulsion”, Thesis, University of Stuttgart (2013).
11. S.I. Anisimov et al., “Electron emission from metal surfaces exposed to ultra short laser pulses”, JETP Letters, vol. 39(2) (1974).
12. D. Bäuerle, Laser Processing and Chemistry, 3. ed., publisher: Springer-Verlag, Berlin, Germany, 2000.
13. M.E. Povarnitsyn et al., “Dynamics of this metal foils irradiated by moderate-contrast high-intensity laser beams”, Physics of Plasmas, vol. 19, 023110 (2012)
14. M.E. Povarnitsyn et al., “A wide-range model for simulation of pump-probe experiments with metals”, Applied Surface Science, vol. 258, pp. 9480–9483 (2012).
15. F. Ercolessi and J. B. Adams, “Interatomic Potentials from First-Principles Calculations: The Force-Matching Method”, Europhysics Letters, vol. 26, pp. 583–588 (1994)
16. B. Hüttner and G. Rohr, “On the theory of ps and sub-ps laser pulse interaction with metals. I. Surface temperature”, Applied Surface Science, vol. 103, pp. 269 – 274 (1996).
17. Z. Lin, V. Zhigilei, and V. Celli, “Electron-phonon coupling and electron heat capacity of metals under conditions of strong electron-phonon nonequilibrium”, Phys. Rev. B, vol. 77 (2008).
18. J. Roth et al., “Laser Ablation of Metals”, in: W. Nagel, D. Kröner, and M. Resch: High Performance Computing in Science and Engineering 2010, Heidelberg, Springer (2010).
19. S. Sonntag, “Computer Simulations of Laser Ablation from Simple Metals to Complex Metallic Alloys”, PhD thesis, University of Stuttgart (2010).
20. C. Ulrich, “Simulation of laser ablation of metals”, Diploma thesis, University of Stuttgart (2007, in German).
21. P. Fromy, C. Deutsch, and G. Maynard, “Thomas-Fermilike and average atom models for dense and hot matter”, *Physics of Plasmas* **3**: 714 – 730 (1996).
22. C. Phipps et al., “Laser impulse coupling at 130 fs”, Applied Surface Science, vol. 252, pp. 4838–4833 (2006).
23. C. Phipps et al., “Review: Laser-Ablation Propulsion”, Journal of Propulsion and Power, vol. 26(4), pp. 609–637 (2010).
24. B. Hüttner, “Femtosecond laser pulse interactions with metals”, in: R. Hull et al. (eds.), The Theory of Laser Materials Processing**,** *Springer Series in Materials Science* **119**: 315 – 337 (2009), Springer
25. R. Ramis et al., “MULTI-fs – A Computer Code for Laser-Plasma Interaction in the Femtosecond Regime“, Computer Physics Communications, vol. 183(3), pp. 637-655 (2012).
26. S. Kato et al., “Numerical simulation of shockwave by KrF laser ablation”, Proc. of SPIE, vol. 4424, pp. 260 (2001).